

1 **Teleconnected Ocean Forcing of Western North American Droughts and Pluvials**
2 **During the Last Millennium**

3 Cody C. Routson ^{a,*}, Connie A. Woodhouse ^{b,c,d}, Jonathan T. Overpeck ^{b,e,f}, Julio L.
4 Betancourt ^g, and Nicholas P. McKay ^a

5 ^aSchool of Earth Sciences and Environmental Sustainability, Northern Arizona
6 University, Flagstaff, AZ, USA, 86011.

7 ^bDepartment of Geosciences, University of Arizona, Tucson, AZ, USA, 85721.

8 ^cLaboratory of Tree-Ring Research, University of Arizona, Tucson, Arizona, USA,
9 85721.

10 ^dSchool of Geography and Development, University of Arizona, Tucson, AZ, USA,
11 85721.

12 ^eInstitute of the Environment, University of Arizona, Tucson, AZ, USA, 85721.

13 ^fDepartment of Atmospheric Sciences, University of Arizona, Tucson, AZ, USA.

14 ^gNational Research Program, Water Mission Area, U.S. Geological Survey, Reston, VA,
15 USA, 20192.

16 *Corresponding author: Cody.Routson@nau.edu, (928) 899-5086, PO Box 4099, 625 S
17 Knoles Dr, Building 12, Rm 100, Flagstaff, AZ 86011-4099

18

19 **Key Words:** Western North America; Drought; Pluvial; Synthesis; Climate Change;

20 Multi-proxy

21

22

Abbreviations list: Western North America (WNA), Sea Surface Temperature (SST), Medieval Climate Anomaly (MCA), El Niño Southern Oscillation (ENSO), Pacific Decadal Oscillation (PDO), Atlantic Multidecadal Oscillation (AMO), Northern Hemisphere annular mode (NAM), Palmer Drought Severity Index (PDSI), North American Drought Atlas (NADA).

23 **Abstract** —Western North America (WNA) is rich in hydroclimatereconstructions,
24 yetquestions remain about the causes of decadal-to-multidecadal hydroclimatevariability.
25 Teleconnection patterns preserved in annually-resolved tree-ring reconstructed drought
26 maps, and anomalies in a global network of proxy sea surface temperature (SST)
27 reconstructions,were used to reassess the evidence linking ocean forcing to WNA
28 hydroclimate variability over the past millennium. Potential forcing mechanisms of the
29 Medieval Climate Anomaly (MCA)and individual drought and pluvial events—including
30 two multidecadal-length MCA pluvials—were evaluated. We show strongteleconnection
31 patterns occurred duringthe driest (wettest) years within persistent droughts(pluvials),
32 implicating SSTs as a potent hydroclimate forcing mechanism. The role of the SSTson
33 longer timescalesismore complex. Pacific teleconnection patterns show little long-term
34 change, whereas low-resolution SST reconstructions vary over decades to centuries.
35 While weaker than the tropical Pacificteleconnections, North Atlanticteleconnection
36 patterns and SST reconstructions also show links to WNA droughts and pluvials, and
37 may in part account for longer-term WNAhydroclimate changes. Nonetheless, evidence
38 linking WNA hydroclimate to SSTs still remainssparse andnuanced—especially over
39 long-timescales with a broader range ofhydroclimatic variability than characterized
40 during the 20th century.

41

42 **1. Introduction**

43 Annually resolved tree-ring records have shown that Western North America
44 (WNA) has experienced a wide range of hydroclimatic conditions over the past
45 millennium. Most remarkable has been the occurrence of megadroughts:multidecadal-

46 length droughts more persistent than any observed during the instrumental record
47 (Woodhouse and Overpeck, 1998). Megadroughts, defined as prolonged drought lasting
48 more than two decades, occurred throughout the last millennium, but were more
49 frequent during the Medieval Climate Anomaly (MCA, ~900-1400 AD), (Cook et al.,
50 2004, 2007, 2010; Meko et al., 2007; Routson et al., 2011; Woodhouse and
51 Overpeck, 1998). Multidecadal-length pluvials, or megapluvials, are also documented
52 throughout the last millennium, but have received less attention than megadroughts
53 despite their comparable societal importance. Here, we reassess the evidence linking
54 these past WNA megapluvials and megadroughts to global sea surface temperature (SST)
55 variations.

56 Observational records (up to ~100 years), document strong causal linkages known
57 as teleconnections between SSTs and WNA climate (e.g., Cayan et al., 1999; Cook et al.,
58 2010; Kam et al., 2014; McCabe et al., 2004, 2008; Tootle et al., 2005; Wang et al.,
59 2008). Because ocean-driven SSTs have a longer memory or persistence than the
60 atmosphere alone, SST variability is the most likely cause of persistent multidecadal-to-
61 centennial hydroclimate variability. WNA climate is strongly connected to SSTs in the
62 tropical Pacific, as characterized by the impact of the El Niño Southern Oscillation
63 (ENSO) (Redmond and Koch 1991). During La Niña events, cool conditions in the
64 eastern equatorial Pacific tend to displace westerly, mid-latitude, storm tracks northward,
65 resulting in reduced cool season precipitation in southwestern North America (e.g., Cayan
66 et al., 1999; Redmond and Koch 1991; Schubert et al., 2009). The opposite tends to be
67 true for El Niño events. Persistent ENSO conditions have been linked to decadal-scale
68 WNA hydroclimate variability over the past ~150 years (Seager et al., 2005). On decadal

69 to multidecadaltimescales, the Pacific Decadal Oscillation (PDO) reflects the dominant
70 mode of SST in the North Pacific (Mantua et al., 1997).Linked with tropical Pacific
71 variability (Newman et al., 2003), the PDO also has demonstrated connections with
72 WNA climate (McCabe et al., 2004, 2008; Tootle et al., 2005). The Indian Ocean works
73 in concert with the Pacific whereby warming in the western Pacific and Indian oceans
74 drives deep atmospheric convection that influences the rising limb of the Walker Cell,
75 and ultimatelyaffecting the mean position of storm tracks and WNA cool season rainfall
76 (Wang et al., 2008). ENSO, PDO, and Indian Ocean all tend to modulate antiphased
77 precipitation in a well-known dipole between southwestern (Southwest) andnorthwestern
78 North America (Northwest).

79 North Atlantic SSTs, as characterized by the Atlantic Multidecadal Oscillation
80 (AMO), may also influence WNA drought, although less directly and to a lesser degree
81 than the Pacific (Cook et al., 2010; Feng et al., 2010; Kam et al., 2014; McCabe et al.,
82 2004;McCabe and Wolock, 2014;Schubert et al., 2009; Tootle et al., 2005). Warm North
83 Atlantic SSTs are associated with warmer WNA temperatures. Regional warming
84 associated with a positive AMO was shown to decrease runoff efficiency and streamflow
85 in the Upper Colorado River Basin (Nowak et al., 2012). The impact of the North
86 Atlantic may not be limited, however, to regional temperature effects on the water cycle
87 (Feng et al., 2010; Kam et al., 2014; McCabe et al., 2004; Schubert et al., 2009). Pacific
88 forcing appears to influence atmospheric circulation patterns driven by the AMO during
89 some seasons (Hu and Feng 2012).Instrumental records and climate models also suggest
90 the largest precipitation anomalies in WNA tend to occur when Pacific and Atlantic SSTs
91 are opposite in sign (Feng et al., 2010; Kam et al., 2014; McCabe et al., 2004, 2008;

92 Schubert et al., 2009), reflecting a combined influence of ocean basins on global
93 atmospheric circulation.

94 The inference that past megadroughts were caused by an extension or
95 enhancement of the processes influencing WNA climate today is prevalent in the
96 literature, although the proposed mechanisms driving this inference vary. The
97 predominant hypothesis is that tropical Pacific SSTs drove sustained WNA aridity, in
98 which extended La Niña-like conditions forced medieval megadroughts (e.g., Conroy et
99 al., 2009a; Graham et al., 2007; Herweijer et al., 2007; Seager et al., 2007; Stahle et al.,
100 2000). Links also have been drawn between the AMO and past WNA drought over the
101 past ~500 years as established by tree rings (Gray et al., 2004; Hidalgo, 2004). North
102 Atlantic SSTs are less well-constrained before ~1500 AD, but some SST proxy records
103 indicate tenuous multidecadal to centennial-scale relationships between North American
104 climate and the North Atlantic (Conroy et al., 2009a; Feng et al., 2008, 2010; Oglesby et
105 al., 2012).

106 Various general circulation model studies support the paleoclimatic evidence and
107 interpretations for the causes of megadroughts. A cool tropical Pacific has been shown to
108 simulate WNA megadroughts in several studies (Burgman et al., 2010; Graham et al.,
109 2007; Seager et al., 2008), and some modeling results indicate a warm North Atlantic
110 plays a role in modulating drought in the Southwest and Midwest (e.g., Feng et al., 2010;
111 Oglesby et al., 2012). Some evidence suggests that ocean teleconnections with recent
112 North American droughts may be weakening, while atmospheric teleconnections are
113 strengthening (Kam et al., 2014; Kumar et al., 2013; Seager et al., 2014; Wang et al.,
114 2014). Though this recent shift may be related to greenhouse warming, it is conceivable

115 that similar shifts, from oceanic to atmospheric controls of North American droughts and
116 pluvials, also have happened in the past.

117 Traditionally, most paleoclimatic studies have focused on the causes of WNA
118 megadroughts over megapluvials, and have not fully evaluated the associations of both to
119 global SST anomalies over past millennium. For example, because background
120 conditions may vary at longer time scales, the drivers for two known pluvials embedded
121 in the generally droughty period of the MCA could differ substantially from those during
122 the wetter post-MCA. Here we extend previous work, using a multiproxy approach to
123 assess the evidence linking SSTs to persistent wet and dry periods in WNA over the past
124 millennium. We use teleconnection patterns embedded in gridded drought reconstructions
125 (Cook et al., 2008), and a screened network of global SST proxy records to explore the
126 following research questions:

127 1) Are differences in WNA hydroclimate between the MCA and post-MCA
128 linked to SSTs? 2) What evidence links WNA megadroughts and megapluvials to SST
129 forcing during the past millennium? 3) Do SST/pluvial associations vary with
130 multidecadal variability, for example, within the MCA?

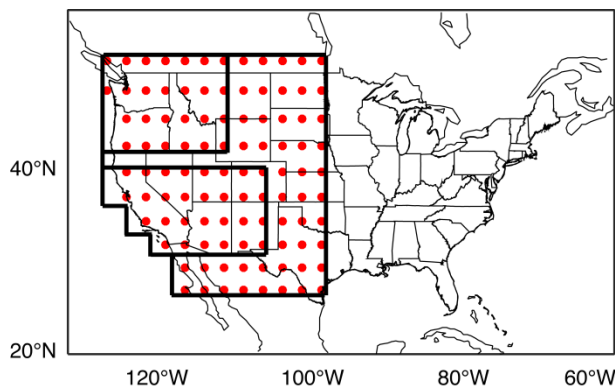
131

132 **2. Materials and Methods**

133 *2.1. Defining Droughts and Pluvials*

134 Droughts and pluvials over the period 900-2006 AD were characterized with the
135 North American Drought Atlas (NADA, Cook et al., 2008). The NADA is a gridded
136 network of tree-ring reconstructed drought as defined by the Palmer Drought Severity
137 Index (PDSI, Palmer, 1965). Although the NADA reconstructed drought metric is

138 summerseason PDSI (Cook et al., 2004), tree rings have inherent seasonal climate
139 sensitivities, and for this reason, the WNA portion of the NADA used here primarily
140 reflects winter precipitation (St. George et al., 2010). PDSI grid points used for WNA
141 (27.5°N to 50° N, 97.5°W to 125°W, after Cook et al., 2004) were averaged and smoothed
142 with a 50-year cubic smoothing spline to highlight regional multidecadal variability (Fig.
143 1). Pluvial and drought periods were identified as intervals during which the smoothed
144 series exceeded 0.2 PDSI units above or below the series mean (-0.17) respectively. This
145 threshold was chosen qualitatively as one that encompasses all relatively severe droughts
146 and pluvials with low frequency components that persisted for multiple decades. We also
147 looked at two subset regions, the Southwest and Northwest (32°N to 40° N, 105°W to
148 115°W and 42°N to 50° N, 110°W to 125°W, respectively, after Cook et al., 2014) for
149 comparison of droughts and pluvials.



150
151 **Fig. 1.** Western North American PDSI reconstruction grid following Cook et al., (2004).
152 The Northwest and Southwest grid subsets are denoted by the respective boxes following
153 the regions used by Cook et al., (2014).

154
155
156

157 *2.2. Teleconnection Patterns*

158 Correlation maps were used to investigate relationships between drought and
159 pluvial patterns and the teleconnections documented by circulation modes. First,
160 instrumental circulation indices for December-February were correlated with each grid-
161 point in the NADA to develop modern teleconnection pattern maps. The December-
162 February season was used because the teleconnections tend to be strongest in the cool
163 season, which also coincides with the seasonality of the WNA tree-ring reconstructed
164 PDSI (St. George et al., 2010). The circulation indices used were the NINO3 index
165 (1856-2006; EXTENDED NINO3 index: Kaplan et al., 1998; Reynolds et al., 2002), the
166 PDO index (1900-2006; Mantua et al., 1997) and the AMO index (1880-2006; van
167 Oldenborgh et al., 2009). The modern teleconnection pattern maps were then spatially
168 correlated with the gridded reconstructed PDSI for every year in the 900–2006 AD
169 analysis period. This resulted in WNA teleconnection pattern strength time series for
170 each of three circulation indices. For example, for NINO3, the time series reflects the
171 strength of the relationship between the modern ENSO/drought spatial pattern and spatial
172 pattern of drought for each year of reconstructed gridded PDSI; the time series is the
173 correlation between the two patterns for each year. Both the modern teleconnection maps
174 and their spatial correlations with gridded PDSI over the past millennia were developed
175 by using the entire set of North American gridded PDSI, not the just subset used to define
176 Western droughts and pluvials. We assessed the teleconnection time series during
177 pluvials and droughts (as defined above, based on smoothed WNA time series), and for
178 the individual wet years and dry years within pluvials and droughts. The wet and dry

179 years were defined by unsmoothed WNA average PDSI deviations exceeding ± 1
180 respectively (e.g., Cook et al., 2007).

181 An important caveat of this method should be noted: because teleconnection
182 patterns are non-stationary (e.g., Batehup et al., 2015; Cole and Cook, 1998; Hu and Feng,
183 2001, McCabe and Dettinger, 1999), this method produces only a rough estimate of the
184 association between these modes of circulation and past WNA climate variability. The
185 goal here is to document variability in the strength of the teleconnections over time, not
186 to reconstruct the respective circulation modes. The teleconnection patterns themselves
187 may be generally indicative of the role of Pacific and Atlantic SSTs, particularly at the
188 spatial scale considered here, and used to help assess potential SST forcing mechanisms
189 of WNA drought variability.

190

191 *2.3 Spectral Analysis*

192 We calculated power spectra, by using the multi taper method (Thomson, 1982) on
193 the tree-ring reconstructed PDSI and teleconnection time series, to test if low-frequency
194 characteristics of the PDSI—that is the persistence of droughts and pluvials—during the
195 MCA (e.g., Herweijer et al., 2007) can be attributed to changes in a particular
196 teleconnection pattern and associated ocean basin. The series were normalized by their
197 mean and variance and detrended prior to spectral analysis. The time series were split
198 into MCA (900-1400 AD) and post-MCA (1400-2000 AD) segments. The 95%
199 significance test for spectral peaks was developed by using a Monte Carlo approach:
200 spectra were computed on 5000 random series with the same AR1 autocorrelation and

201 variance as the original series. The upper 95th percentile for each distribution was used as
202 the confidence limit for testing significance.

203

204 *2.4. PaleoSST Reconstruction Anomaly Maps*

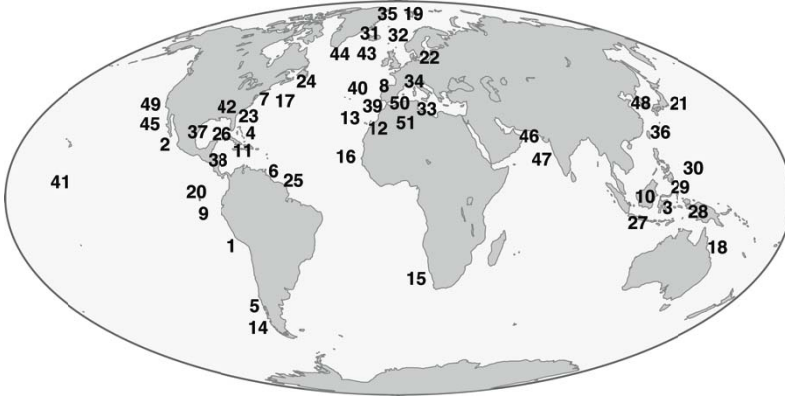
205 To further investigate links between WNA climate and SST forcing, we
206 assessed proxy SST reconstructions. The SST reconstructions, based on marine proxy
207 records, provide direct observations of the potential drought and pluvial forcing
208 mechanisms. Although there are limitations with these records as discussed below, the
209 SST reconstructions provide an independent test of ocean background conditions over
210 long MCA to post-MCA timescales, and (albeit less reliably) during multidecadal-scale
211 drought and pluvial events.

212 The SST records were obtained from the Expanded Global Holocene Spatial and
213 Temporal Climate Variability database (Leduc et al., 2010a), NOAA's paleoclimate
214 database (<http://www.ncdc.noaa.gov/paleo/paleo.html>), the PANGEA data library
215 (<http://www.pangaea.de>), or digitized from the publication when not in public
216 repositories and when authors did not respond to our data requests. Proxy SST records
217 were screened by resolution and age control. Records were retained with 20 or more data
218 points in the analysis period, and two or more age control points in the analysis period
219 (900-2006 AD). For the drought and pluvial analysis, records were retained with data
220 points in at least two drought or two pluvial intervals, respectively. A total of 51 records
221 passed the screening (Fig. 2. Table 1). To assess potential relationships between SSTs
222 and past WNA climate, we evaluated proxy SST anomalies for MCA and post-MCA
223 periods, and for drought and pluvial intervals. Proxy SST anomalies were computed with

224 respect to the 900-2006AD mean, or series length mean, if shorter than the analysis
225 period.

226 It is important to note the limitations of using proxy SST reconstructions to assess
227 ocean surface temperature patterns during drought and pluvial events. The first
228 uncertainty is the seasonal dependency of some SST proxies (e.g., Leduc et al., 2010a),
229 whereby theseasonality'sthe SST proxies are not necessarily aligned with those of the
230 circulation modes. A second limitation is that theSST proxy resolution is lower, with
231 greater dating uncertainty, than the tree-ring reconstructed PDSI. Thus, the proxy SST
232 reconstructions reflect variability over long time-scales (decadal to centennial), whereas
233 tree-ring records preserve predominantly annual-to-decadal-scale variability (e.g., Cook
234 et al., 1995). Consequently, the SST anomaly maps are not reflecting the same time-scales
235 of variability as the tree-ring drought records, and assessing the influence of SST
236 anomalies for relatively short, individual drought and pluvial intervals is unlikely to
237 provide meaningful constraints. To help alleviate the resolution and dating uncertainty
238 mismatch, we analyzed a composite of all drought and pluvial intervals to average out
239 some dating uncertainty in the SST records and assess general relationships. Nonetheless,
240 the proxy SST anomaly maps characterize long-term (multi-century-scale) changes in the
241 oceans, and droughts and pluvials that are driven by relatively short term anomalies in
242 SST patterns will not be apparent in this analysis.

243



245

247 **Fig. 2.** Proxy sea surface temperature record site location key. Site numbers correspond
 248 with records in Table 1 and corresponding supplemental dataset.

248

249 *2.5. Additional evidence*

256 We employ several other sources of evidence of past WNA drought and pluvial
 257 forcing mechanisms, including several tropical precipitation reconstructions as indicators
 258 of tropical Pacific SST variability. We also evaluate the dominant modes of the NADA as
 259 characterized by Woodhouse et al. (2009), to assess the potential causes of the MCA
 260 pluvials. They defined two dominant modes of North American drought by using
 261 principal components analysis, that are linked to ENSO and the Northern Hemisphere
 262 annular mode (NAM) respectively.

256 **Table 1.** Proxy SST records including location, reference, resolution, and age control used in this analysis. Records are available in
 257 the associated supplemental dataset.

#	Core Name	Reference	Lat (°N)	Lon (°E)	Resolution: mean (min max) yr/smpl	Proxy	Dating Method	# of 14C	# of 210PB	Total Tie points
1	B0406	Gutierrez et al. (2011)	-14.13	-76.50	2.7 (1-7)	Alkenone	210Pb, AMS 14C	6	4	10
2	BC-43	Goni et al. (2006)	27.90	-111.66	4.6 (4-13)	Alkenone	210PB, varve		59	59
3	BJ8-03-32GGC	Oppo et al. (2009)	-3.53	119.27	10 (10-10)	Mg/Ca	210Pb, AMS 14C, Tephra	5.0	13.0	19.0
4	Bahamas Coral	Saenger et al. (2009)	25.84	-78.62	1 (1-1)	Coral	U/Th, annual growth bands			7+band chron
5	CF7-PC33	Sepulveda et al. (2009)	-44.33	-72.97	20.4 (8-49)	Alkenone	AMS 14C	4		4
6	PL07-73	Black et al. (2007)	10.75	-64.77	1.4 (0.5-2.6)	Mg/Ca	Varve, 210Pb, AMS 14C	12	30	42+varve chron
7	MD99-2209	Cronin et al. (2003)	37.82	-76.12	3.2 (1-34.7)	Mg/Ca	137Cs, 210Pb, AMS 14C	9	Multiple Cores	9+
8	D13882	Rodrigues et al. (2009)	38.63	-9.45	22.4 (21-44)	Alkenone	AMS 14C	1		1
9	El Junco	Conroy et al. (2009b)	-0.90	-89.48	5.5 (1-9)	Diatom	137Cs, 210Pb, AMS 14C	4	9	14
10	GGC13	Linsley et al. (2010)	-7.40	115.20	33 (23-35)	Mg/Ca	AMS 14C	1		1
11	79GGC	Lund and Curry (2006)	24.36	-83.35	22.9 (9-104.8)	Mg/Ca	AMS 14C	3		3
12	GeoB6007-2	Kim et al. (2004)	30.85	-10.27	31.1 (31-32)	Alkenone	AMS 14C	1		1
13	GeoB6008-6	McGregor et al. (2007)	30.85	-10.10	7.9 (0.5-13)	Alkenone	210Pb, AMS 14C	3	15	18
14	GeoB71863	Mohtadi et al. (2007)	-44.15	-75.16	51.4 (19.2-99)	Alkenone	AMS 14C	3		3
15	GeoB8331-4	Leduc et al. (2010b)	-29.14	16.72	21.9 (19-33)	Alkenone	210Pb, AMS 14C	1	17	18
16	GeoB9501-5	Kuhnert and Mulitza (2011)	16.84	-16.73	9.4 (5-28)	Mg/Ca	AMS 14C	2		2
17	Gulf of Maine Shells	Wanamaker et al. (2007)	43.65	-69.80	3 (1-394)	Bivalves	Annual band counting, AMS 14C	3		3 + layer chron
18	Barrier Reef Coral	Hendy et al. (2002)	-18.33	146.45	5.1 (5-10)	Coral Sr/Ca	annual growth bands			band chron
19	JM-06-WP-04-MCB	Bonnet et al. (2010)	78.92	6.77	39.7 (15.3-85.6)	dinocyst taxa	137Cs, 210Pb, AMS 14C	2	9	12
20	KNR195-5	Rustic et al. (2015)	1.25	-89.69	45.4 (26.5-81)	Mg/Ca	AMS 14C	3		3
21	KR02-06A	Isono et al. (2009)	36.03	141.78	24.3 (11-53)	Alkenone	AMS 14C	3		3
22	M200309/ENAM9606	Richter et al. (2009)	55.65	13.99	17.4 (11-37)	Mg/Ca	226Ra, 137Cs, 210Pb, AMS 14C	4	13	17
23	118MC-A	Lund and Curry. (2006)	24.59	-79.27	24.6 (22.5-25.7)	Mg/Ca	AMS 14C	2		2
24	MC-29D	Keigwin et al. (2003)	45.89	-62.80	26.8 (7.9-53)	Alkenone	210Pb, AMS 14C	2	11	13
25	MC4	Goni et al. (2006)	10.65	-64.66	7.7 (2-23)	Alkenone	210Pb, AMS 14C, varve			varve chron
26	62MC-A	Lund and Curry (2006)	24.33	-83.26	26.6 (11-50)	Mg/Ca	AMS 14C	2		2

27	MD98-2160	Newton et al. (2006)	-5.20	117.48	7.5 (1-20)	Mg/Ca	AMS 14C, Tephra	3		4
28	MD98-2176	Stott et al. (2004)	-5.00	133.44	27.2 (10-66)	Mg/Ca	AMS 14C	2		2
29	MD98-2177	Newton et al. (2011)	1.40	119.08	12.2 (10.9-21.8)	Mg/Ca	AMS 14C	2		2
30	MD98-2181	Stott et al. (2004)	6.30	125.82	19.7 (2-88)	Mg/Ca	AMS 14C	5		5
31	MD99-2275	Sicre et al. (2008);(2011)	66.56	-17.70	3.2 (1-6)	Alkenone	Tephra Chronology, 210pb		23	28
32	MD99-2275	Eiriksson et al. (2006)	66.56	-8.00	15.3 (3.3-27.2)	Diatom	AMS 14C, Tephra Chronology	7		11
33	MINMC06-1a	Moreno et al. (2012)	40.50	4.03	34.7 (11-70)	Alkenone + Mg/Ca	AMS 14C	4		4
34	MINMC06-1b	Moreno et al. (2012)	40.50	4.03	37.8 (11.7-70)	Alkenone + Mg/Ca	AMS 14C	4		4
35	MSM5/5-712	Spielhagen et al. (2011)	78.91	6.77	35.8 (18-54)	Forams	AMS 14C	3		3
36	ODP-1202B	Wu et al. (2012)	24.80	122.50	28.2 (13-104)	Tex86	AMS 14C	2		2
37	PE07-2	Richey et al. (2009)	26.68	-93.93	23.2 (11.8-33.1)	Mg/Ca	AMS 14C	3		3
38	PE07-5I	Richey et al. (2009)	27.55	-92.17	18.8 (18.8-8.8)	Mg/Ca	AMS 14C	3		3
39	PO287-26	Rodrigues et al. (2009)	38.33	-9.21	11.8 (3-85)	Alkenone	210Pb, AMS 14C	6	12	18
40	PO287-26-2	Abrantes et al. (2005)	38.56	-9.35	9 (1-161)	Alkenone	210Pb, AMS 14C	1		1+ cross correlation
41	Palmyra	Cobb et al. (2003)	6.00	-160.00	2.5 (1-189)	Coral	U/Th			25
42	PigmyBasin	Richey et al. (2007)	27.20	-91.42	13.3 (12.3-37)	Mg/Ca	AMS 14C	5		5+varve chron
43	RAPid-21-3K	Sicre et al. (2011)	57.45	-27.91	10.4 (10-30)	Alkenone	AMS 14C	5		5+varve chron
44	Rapid-21	Miettinen et al. (2012)	57.27	-27.54	5.6 (1-21)	Diatom	210Pb, AMS 14C	9	5	14
45	SABA8772 and SABA8871	Hendy et al. (2013); Zhao et al. (2000); Schimmelmann et al. (2013)	34.23	-120.02	1.2 (0.1-8.2)	Alkenone	AMS 14C and Varve	25		25+varve chron
46	SO90-39KG	Doose-Rolinski et al. (2001)	24.83	65.92	16.5 (1-46)	Alkenone	Varve and AMS 14C	5		5+varve chron
47	SO13-0275KL	Doose-Rolinski et al. (2001)	24.83	65.92	11.2 (6-29)	Alkenone	Varve and AMS 14C	5		5+varve chron
48	SSDP-102	Kim et al. (2004)	34.95	128.88	45 (15-78)		AMS 14C	3		3
49	ODP893A	Kennett and Kennett (2000)	34.29	-120.04	28.8 (10.1-96.1)	Mg/Ca	AMS 14C	11		11
50	436B	Nieto-Moreno et al. (2013)	36.21	-4.31	30 (6-65)	Tex86, Alkenone, BIT	210Pb, AMS 14C	2	10	12
51	384B	Nieto-Moreno et al. (2013)	35.99	-4.75	38.9 (6-66)	Tex86, Alkenone, BIT	210Pb, AMS 14C	2	10	12

258

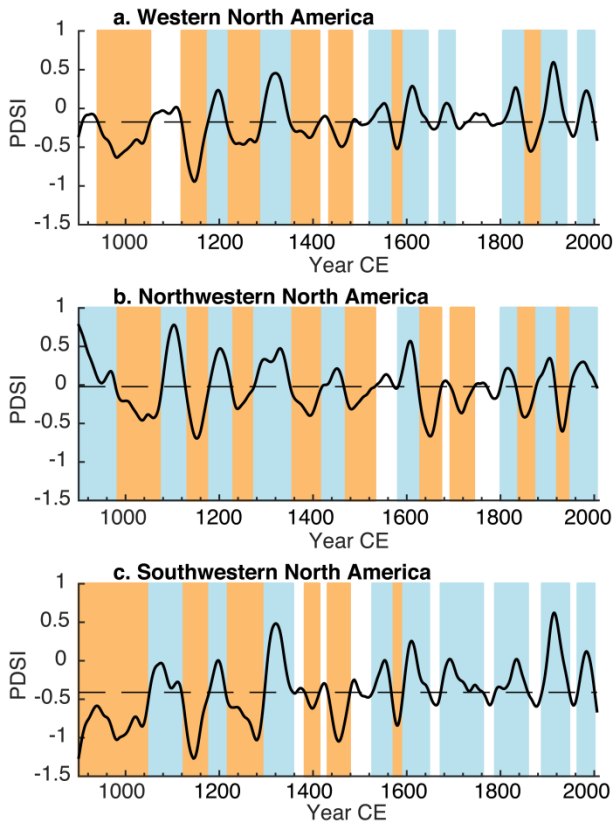
259

260

261 **3. Results**

262 *3.1. Drought and Pluvial Events*

263 Smoothed WNA PDSI characterizes seven persistent droughts and eight persistent
264 pluvials between 900 and 2000 AD (Fig. 3a, Table 2). The WNA droughts occurred
265 predominantly in the MCA whereas pluvials were more concentrated in the post-MCA
266 period. Two persistent WNA pluvials, however, occurred in the MCA and two
267 persistent droughts occurred in the post-MCA. The widespread drought and pluvial events
268 primarily reflect events that span WNA, including regions with somewhat different (and
269 sometimes opposing) teleconnections. Pluvials and droughts for the Northwest and
270 Southwest show strong coherence through the MCA, but major differences after about
271 1400 (Fig. 3b and c). Whereas a number of the pluvials are shared in the two regions over
272 the post-MCA period, the patterns of droughts are not. This suggests that large-scale
273 drivers of pluvials and drought were dominant in the MCA, influencing the entire region
274 in the same way, whereas regional-scale drivers were more important after this period.
275 Because of this common variability on longer timescales, in this study we focused on
276 westwide patterns of droughts and pluvials.
277



278

279 **Fig. 3.**Characterizing droughts and pluvials. Time series of averaged PDSI gridpoints for
 280 a) western North America, b) northwestern North America, and c) southwestern North
 281 America, spanning 900-2006 AD, and smoothed with a 50-yr cubic smoothing spline.
 282 Droughts and pluvials are shown in brown and blue respectively.

283

284 **Table 2.** Drought and pluvial intervals for WNA.

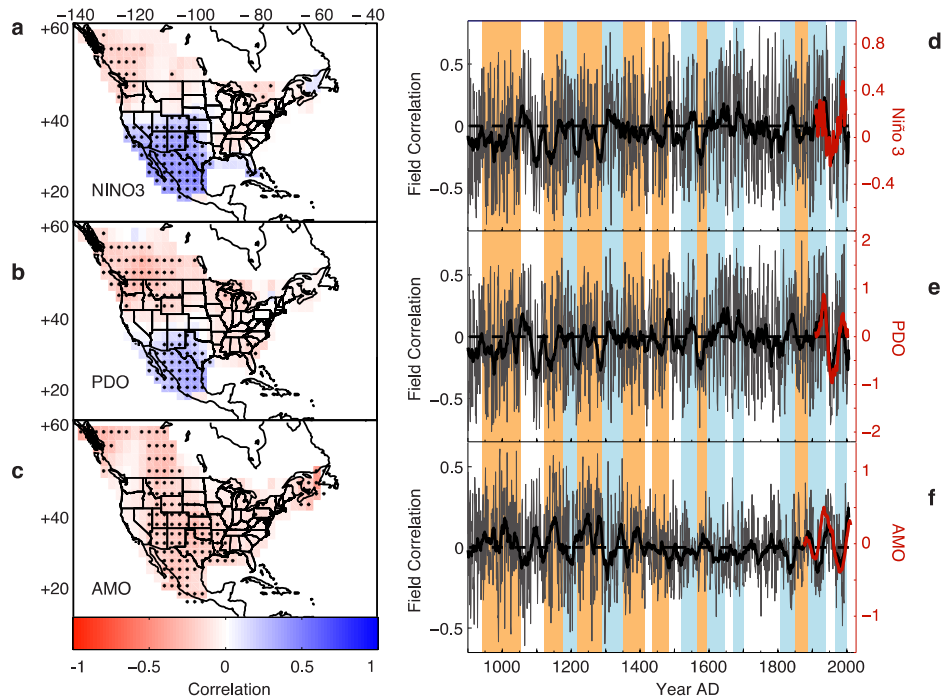
WNA Drought intervals (CE)	WNA Pluvial intervals (CE)
941-1052	1176-1215
1120-1175	1290-1350
1216-1289	1521-1565
1351-1413	1594-1644
1435-1483	1670-1702
1566-1593	1806-1848
1849-1888	1889-1940

285

286

287 *3.2. Teleconnection Patterns*

288 The teleconnection pattern maps documenting the correlations between
289 instrumental circulation indices and North American PDSI are shown in Figures 4a-c and
290 are similar to those shown in Cook et al., (2014). The NINO3 and PDO teleconnection
291 maps are characterized by a north-south dipole in WNA climate: when the Southwest is
292 dry, the Northwest is wet and vice versa (Fig. 4a-b). The NINO3 teleconnection pattern is
293 stronger and more widespread in the Southwest, whereas the PDO has a stronger
294 signature in the Northwest. Nonetheless, spatial teleconnection patterns of the PDO and
295 NINO3 in WNA are extremely similar. The modern relationship between the AMO and
296 WNA climate is less pronounced. The AMO has a weakly negative but significant
297 relationship with PDSI across much of North America during the instrumental period
298 (Fig. 4c).



299

300 **Fig. 4.** Teleconnection pattern analysis. Maps (a-c) show the modern teleconnection
 301 relationship (correlation fields) between instrumental climate modes including NINO3,
 302 PDO, and the AMO and the last ~100 years of the NADA respectively. Negative
 303 correlations are in red and positive correlations are in blue. Black dots indicate local grid
 304 correlation significance ($p \leq 0.1$). The time series (d-f) show spatial correlation values
 305 between the maps (left) and annual tree-ring reconstructed PDSI patterns in the
 306 NADA over the past millennium. The heavy black lines are smoothed with a 20 year
 307 moving average. The instrumental climate modes smoothed with a 20 year moving
 308 average are plotted on the teleconnection strength time series in red. The vertical brown
 309 and blue bars reflect the drought and pluvial events in WNA respectively.

310

311 Correlating the teleconnection maps with the annual reconstructed NADA maps
312 over the 900–2000 AD analysis period results in time series of r-values, indicating the
313 strength and sign of the teleconnection patterns through time (Fig. 4d-f). The NINO3
314 teleconnection time series (Fig. 4d) ranges between $r = 0.81$ and $r = -0.80$ with a mean
315 absolute teleconnection strength of $r = 0.32$. The PDO teleconnection time series (Fig. 4e)
316 ranges between $r = 0.76$ and $r = -0.77$ with a mean absolute teleconnection strength of $r =$
317 0.30 . Not surprisingly the PDO and NINO3 teleconnection time series are nearly identical
318 to each other ($r = 0.96$, $p < 0.0001$), as reflected by their teleconnection patterns. As a
319 result, distinguishing between the NINO3 and PDO patterns is not feasible. Correlations
320 between the AMO teleconnection pattern and WNA PDSI are weaker (Fig. 4f), and range
321 between $r = \pm 0.61$ with a mean absolute teleconnection strength of $r = 0.18$. The NINO3
322 and AMO teleconnection series are negatively correlated with each other ($r = -0.57$, $p <$
323 0.0001), as are the PDO and AMO teleconnection time series ($r = -0.57$, $p < 0.0001$). The
324 NINO3 teleconnection series has the strongest relationship with WNA PDSI ($r = 0.77$),
325 followed by the PDO teleconnection series (0.55) and the AMO teleconnection series ($-$
326 0.43).

327 The teleconnection patterns are not markedly different in the MCA and Post-
328 MCA in WNA. Negative (La Niña) NINO3 teleconnection patterns are slightly more
329 frequent during the MCA (59% of all years) than the post MCA (53% of all years). The
330 average absolute strength of the NINO3 teleconnection pattern series does not change
331 between the MCA ($r_{\text{abs}} = 0.32$) and post-MCA ($r_{\text{abs}} = 0.31$). The frequency of
332 positive/negative AMO teleconnection patterns changes slightly between the MCA and
333 post MCA (positive AMO in 54% of all years during the MCA and 45% of all years in

334 the post MCA). The average absolute AMO teleconnection pattern strength also increases
335 during the MCA ($r_{abs} = 0.22$) with respect to the post-MCA ($r_{abs} = 0.14$).

336 Mean teleconnection patterns do not show strong differences between droughts
337 and pluvials. During droughts, the teleconnection series strength averages for NINO3,
338 PDO, and AMO are -0.11, -0.07, and 0.04, respectively. During pluvials, the values for
339 NINO3, PDO, and AMO are 0.02, 0.03, and -0.04, respectively. However, persistent
340 pluvials and droughts contain years that represent breaks in these persistent conditions.
341 For example, the 12th century drought in the upper Colorado River Basin that persisted
342 for six decades contained about a dozen above average flow years (Meko et al. 2007).
343 NADA maps show that individual anomalous dry or wet years within decadal-scale
344 droughts and pluvials respectively have much stronger teleconnection patterns than the
345 overall events, suggesting that the teleconnection patterns are more representative of the
346 spatial pattern of interannual variability than of longer timescale phenomena. Figure 5
347 shows histograms of teleconnection correlations with NADA during the wettest pluvial
348 and driest drought years. The dry drought years have average teleconnection strengths of
349 0.39 (NINO3), -0.28 (PDO) and 0.15 (AMO). Wet pluvial years have a weaker
350 teleconnection relationship than dry drought years, with correlations of 0.29 (NINO3),
351 0.21 (PDO), and -0.12 (AMO). Although the signs of the teleconnection pattern
352 relationships are largely consistent with those of the modern period, the distribution of
353 teleconnection pattern values indicates a range in the direction and strength of these
354 relationships even during the extreme years (e.g., Kumar et al., 2013).

355

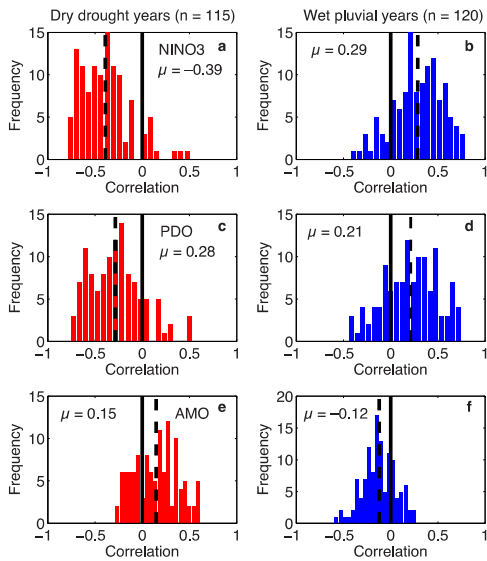


Fig. 5. Teleconnection strength during the driest WNA drought years and the wettest WNA pluvial years. Dry drought years are defined as years with PDSI < -1 during droughts and wet pluvial years as PDSI > 1 during pluvials. Histograms show the frequency of positive and negative teleconnection patterns during these extreme years. Negative ENSO correlations indicate a La Niña type

366 teleconnection pattern. Positive AMO correlations indicate a warm North Atlantic type
 367 teleconnection pattern. The solid vertical lines show correlations of zero and the dashed
 368 vertical lines show the mean correlation strengths.

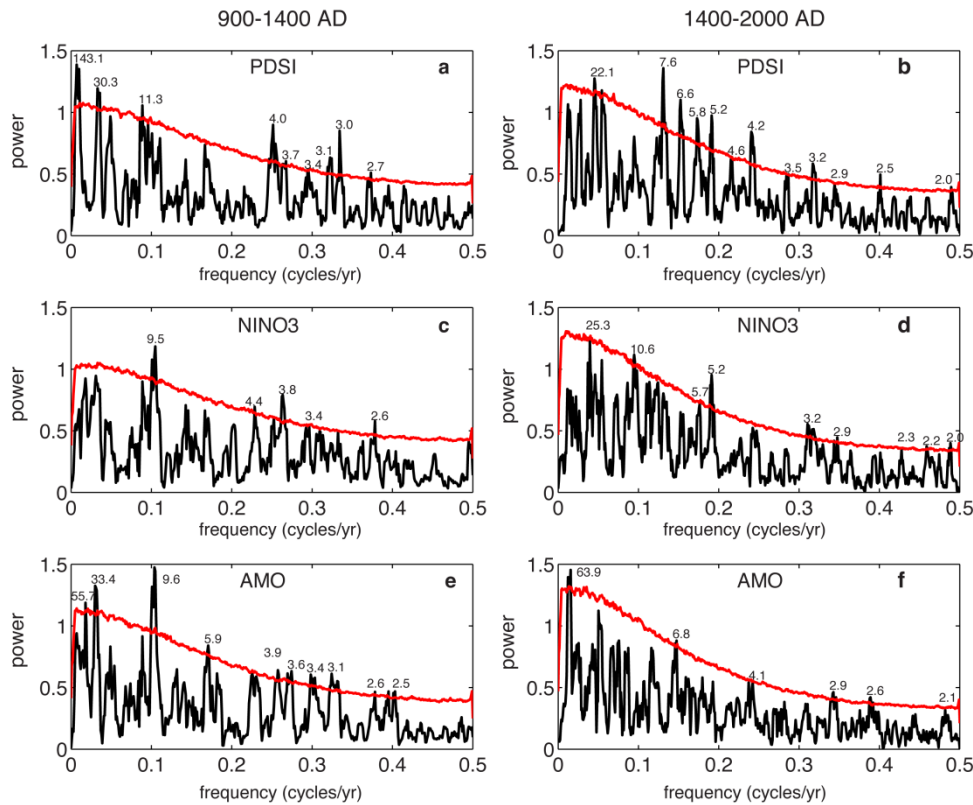
369

370 3.3. Spectral Analysis

371 Spectral analysis shows WNA PDSI has significant spectral peaks around 143,
 372 30, and 11 years, as well as between three and four years, during the MCA (Fig. 6a). In
 373 contrast, the post-MCA period shows greater spectral strength at periods of 4-8 years,
 374 with an additional lower peak at 22 years. (Fig. 6b). Spectral peaks in the teleconnection
 375 series do not correspond with these differences between MCA and post MCA PDSI. The
 376 NINO3 teleconnection series has a significant peak at 9.5 years as well as several at less
 377 than five years during the MCA (Fig. 6c). Post-MCA, the NINO3 has a significant peak at
 378 5.2 years, with a number of other weakly significant peaks (Fig. 6d). During the MCA, the

379 AMO teleconnection series has prominent significant spectral peaks at 33.4 years and 9.6
 380 years, contrasting with a prominent 63.9-year post-MCA AMO spectral peak.

381



382

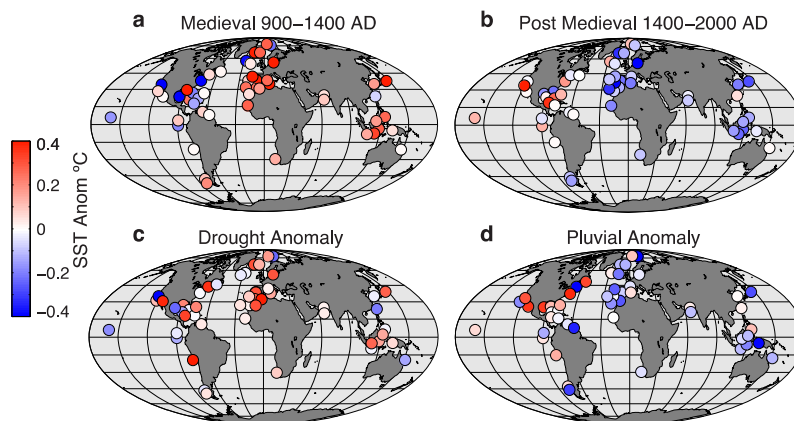
383 **Fig. 6.** Spectral analysis. Power spectra of WNAPDSI (a-b), NINO3 teleconnection series
 384 (c-d), and the AMO teleconnection series (e-f) during the MCA (900-1400 AD, left
 385 panels) and post-MCA (1400-2007 AD, right panels) periods. Peaks significant above the
 386 95% red noise confidence interval (red) are denoted in years.

387

388 3.4. PaleoSST Reconstruction Anomaly Maps

389 This analysis is beginning to push the limits of geochronological accuracy and
 390 resolution for SST reconstructions; nevertheless, general patterns of background SST
 391 patterns emerge in our analysis. The strongest signals for both the MCA/post-MCA and

392 drought/pluvial composites occur in the northeast Atlantic and in the western tropical
393 Pacific. SST anomalies were variable but generally cool during the MCA in the eastern
394 tropical Pacific, warm in the western Pacific, and northern and eastern Atlantic, and
395 variable in the western Atlantic (Fig. 7a). The post-MCA anomalies are a reversal of this
396 pattern (Fig. 7b), which is expected because of how the anomalies were calculated. Both
397 patterns are consistent with a La Niña-like MCA and an El Niño-like post MCA.
398 Combined drought and pluvial periods for WNA also generally have La Niña-like and El
399 Niño-like proxy SST anomalies in the Pacific respectively (Fig. 7c-d). The drought SST
400 anomaly pattern in WNA (Fig. 7c) shows more broad scale warming in the North
401 Atlantic, in contrast to the stronger warm anomalies focused in the northern and eastern
402 Atlantic during the MCA (Fig. 7a). The WNA pluvial pattern shows generally warmer
403 SSTs in the eastern tropical Pacific and Gulf of Mexico and cooler SSTs in the northern
404 and eastern Atlantic and western Pacific (Fig. 7d).
405



406

407 **Fig. 7.** Proxy SST anomaly maps. SST anomalies during(a) the medieval period, (b) the
408 post medieval period. Panels (c-d) show SST anomalies during persistent drought and
409 pluvial events in WNA. Drought and pluvial events are defined by the smoothed series in
410 Fig. 3. Proxy SST anomalies are computed with respect to the 900-2000 AD mean, or the
411 series length mean if shorter than the analysis period.

412

413 **4. Discussion**

414 Teleconnection patterns reflected in the gridded PDSI and proxy SST
415 reconstructions provide a way to examine the SST forcing mechanisms of past WNA
416 climate variability. Below we assess evidence regarding each of the research questions
417 set forth in the introduction.

418

419 *4.1. Are differences in WNA hydroclimate between the MCA and post-MCA linked to*
420 *SSTs?* The MCA has been characterized by widespread and persistent drought in WNA
421 (e.g., Cook et al., 2004; Herweijer et al., 2007; Woodhouse and Overpeck 1998). Here we
422 confirm this characterization, identifying more long-lasting drought events in WNA during
423 the MCA than in post-MCA years (Fig. 3), as well as an increase in low frequency
424 variance of PDSI during the MCA (Fig. 6a). Were these differences in WNA climate
425 forced by ocean/atmosphere circulation patterns related to SSTs?

426 Previous work has attributed the WNA MCA climate to the tropical Pacific (e.g.,
427 Conroy et al., 2009a; Graham et al., 2007; Herweijer et al., 2007; Seager et al., 2007). In
428 this analysis, we show that strong tropical Pacific teleconnection patterns were present
429 throughout the past millennium (Fig. 4a). Yet there was little change in the strength or

430 direction of Pacific teleconnection patterns during the MCA compared to the post-MCA
431 period. In addition, teleconnection patterns do not indicate that stronger or more frequent
432 La Niña events forced MCA megadroughts. Because of the greater frequency of drought
433 in WNA during the MCA, and the correspondence between dry years and La Niña-like
434 conditions, and less drought, along with the relationship between wet years and El Niño-
435 like conditions the reverse for wet years(Fig. 5a and b), this result was somewhat
436 unexpected. Furthermore, spectral analysis of the NINO3 teleconnection series does not
437 show an increase in low-frequency variance coincident with greater persistence in PDSI
438 during the MCA (Fig. 6c).

439 Changes in Atlantic SSTs could be another mechanism forcing the MCA/post-
440 MCA climate differences in WNA. Hidalgo et al. (2004) suggest that much of the low
441 frequency variance in past WNA hydroclimate variability is linked to North Atlantic SST
442 variations related to the AMO. The AMO teleconnection series (Fig. 4f) has a weaker
443 relationship with WNA climate than Pacific teleconnection series ($r = -0.43$ versus $r =$
444 0.77), but the overall AMO teleconnection strength is greater during the MCA. This could
445 indicate the North Atlantic had a stronger influence on WNA climate during the MCA. In
446 modern times the North Atlantic varies on long (60-80 year) timescales. It is possible that
447 a stronger WNA-North Atlantic teleconnection during the MCA could have modulated the
448 timing of droughts and pluvials, as well as the underlying low-frequency climate
449 variability. Spectral analysis of the AMO teleconnection series, however, shows no MCA
450 spectral peaks that correspond with the enhanced low frequency PDSI variability (Fig. 6a
451 and e).

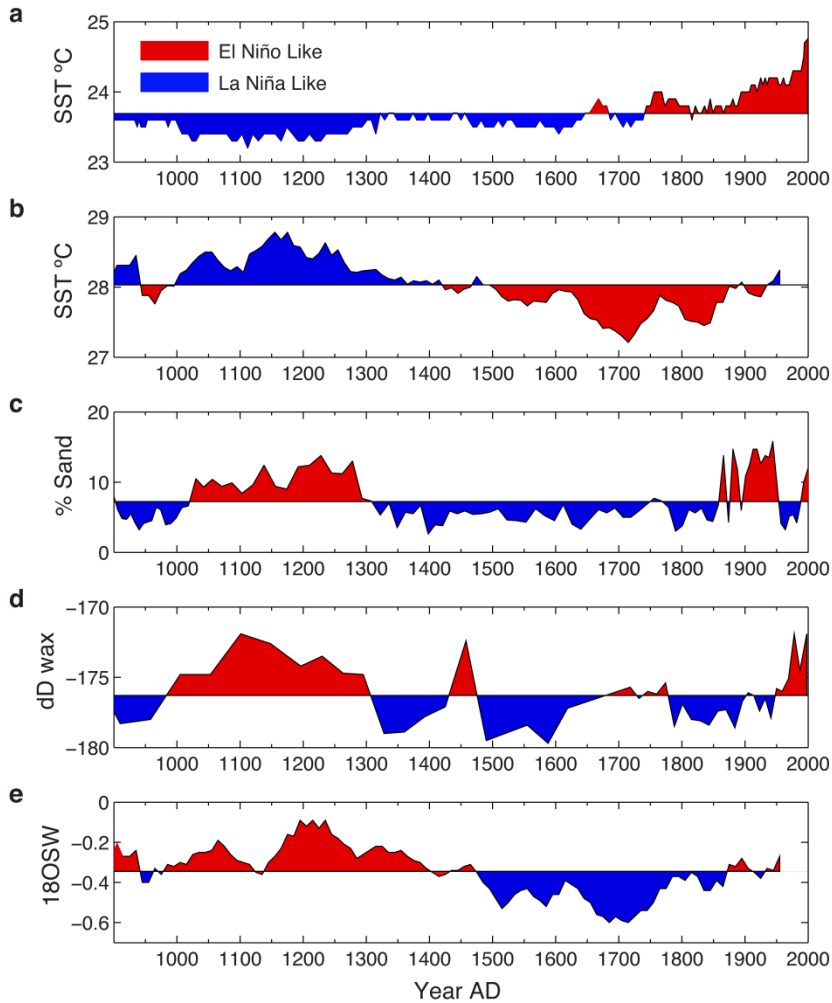
452 In contrast to the tree-ring based WNA teleconnection patterns, proxy SST
453 records, particularly in the western tropical Pacific and eastern North Atlantic, indicate a
454 shift from a warm North Atlantic and La Niña-like Pacific pattern during the MCA to a
455 cool North Atlantic and El Niño-like Pacific pattern during the post-MCA (Fig. 7a-b).
456 These results suggest a La Niña-like based state in SSTs in the MCA. As discussed above,
457 WNA drought patterns show neither an increased strength nor frequency in La Niña
458 teleconnection patterns during the MCA, which is inconsistent with persistent La Niña as
459 a dominant driver for the MCA megadroughts. If La Niña conditions were responsible for
460 the WNA MCA climate, the associated teleconnection may have imparted a different
461 spatial footprint of drought. There is some agreement between North Atlantic
462 teleconnection patterns and the SST proxy records, where warmer Atlantic background
463 MCA SSTs (e.g., Oglesby et al., 2012) coincided with increased AMO teleconnection
464 strength.

465 Prior research results using Pacific precipitation proxy records suggest a more
466 complex La Niña-like MCA story (e.g., Yan et al., 2011). Precipitation reconstructions
467 from the eastern and western tropical Pacific show increases in MCA eastern tropical
468 Pacific runoff intensity (Fig. 8c; Conroy et al., 2008), and decreases in western tropical
469 Pacific rainfall (Fig. 8d; Tierney et al., 2010), which is further supported by an increase in
470 western tropical Pacific sea surface salinity (Fig. 8e, Oppo et al., 2009). These
471 precipitation and salinity conditions are the opposite from what would be expected based
472 on the SST proxy data for the MCA and post MCA periods, with the precipitation
473 records suggesting an El Niño-like MCA and a La Niña-like post-MCA (e.g., Conroy et al.,
474 2010; Oppo et al., 2009; Tierney et al., 2010; Yan et al., 2011). A likely explanation for

475 this enigma may be stronger El Niño events embedded within largely persistent periods
476 of La Niña-like tropical Pacific conditions(e.g., Conroy et al., 2009b; Routson et al.,
477 2011). Yet a record of ENSO variability using $\delta^{18}\text{O}$ from single-shell *G. ruber* in the
478 eastern tropical Pacific indicates less ENSO variance during the MCA (Rustic et al.,
479 2015). Finally, a recent multiproxy ENSO reconstruction shows no clear shift in the
480 background state of the tropical Pacific between the MCA and post-MCA (Emile-Geay et
481 al., 2013). The widely varying evidence suggests that conditions in the tropical Pacific
482 during the MCA may have been complex, with no modern analogue (e.g., Tierney et al.,
483 2010). Nonetheless, proxy observations of SSTs strongly suggest background SSTs during
484 the MCA were La Niña-like followed by El Niño-like post-MCA conditions.

485 Some of the discrepancies between the teleconnection and SST proxy data results
486 may be due to the tree-ring based PDSI teleconnection patterns better reflecting annual to
487 multidecadal variability and the SST proxy data better reflecting century-scale variability.
488 The broad spatial and temporal scale differences between the MCA and post-MCA are
489 more likely to be highlighted by the SST data whereas the variability of PDSI
490 teleconnections within theMCA and post-MCA periods are more strongly represented in
491 the tree-ring data.

492



493

494 **Fig. 8.** Tropical Pacific SST and precipitation ENSO reconstructions in apparent
 495 contradiction. Records are from both sides of the tropical Pacific basin. Red coloring
 496 indicates El Niño-like conditions and blue color indicates La Niña like conditions. a)
 497 Diatom inferred SST from the Lake El Junco in the Galapagos Islands (Conroy et
 498 al., 2009b), b) Mg/Ca inferred SST from the Indo Pacific Warm Pool (Oppo et al., 2009),
 499 c) grain size inferred precipitation intensity from Lake El Junco (Conroy et al., 2008), d)
 500 deuterium leaf wax isotope precipitation reconstruction from the Indo Pacific Warm Pool
 501 (Tierney et al., 2010), and e) $\delta^{18}\text{O}$ of sea water inferred salinity reconstruction from the
 502 Indo Pacific Warm Pool (Oppo et al., 2009).

503

504 *4.2. What evidence links WNA megadroughts and megapluvials to SST forcing during the*
505 *past millennium?*

506 Although the teleconnection patterns do not reflect marked differences between
507 MCA and post MCA period, they do help elucidate the forcing mechanisms associated
508 with individual drought and pluvial events. For example, the late 16th century
509 megadrought stands out, characterized by a correspondence between dry conditions and
510 La Niña patterns between 1566 and 1578, along with a positive AMO. This is in support
511 of the La Niña-forcing mechanism hypothesis for this drought set forth by Stahle
512 (2000). Many of the MCA droughts also have sequences of La Niña-like PDSI patterns,
513 but they tend to not persist through the entire events (e.g., the first half of the 1125-1175
514 drought and the last part of the drought ending in the late 1300s). In a similar way, AMO
515 teleconnections tend to be positive (warm Atlantic SSTs) but variable over the periods of
516 MCA drought. The teleconnection patterns during pluvials were generally weaker than for
517 droughts. Pluvials during the 17th and 18th centuries had sequences of El Niño-like
518 patterns, but the MCA pluvials show a weaker correspondence to El Niño teleconnections.
519 Teleconnection pattern relationships with AMO during pluvials tend to be negative (cool
520 Atlantic) during at least parts of the pluvial periods in both the MCA and post-MCA
521 periods. These variable relationships become stronger when the most extreme wet and dry
522 years are examined (Fig. 5).

523 In examining the relationship between WNA megadroughts and pluvials to SST
524 forcing, the resolution and age control of proxy SST reconstructions, which are much
525 lower than that of the tree-ring based teleconnection patterns, must be considered.

526 Caution is advised when interpreting these records on relatively short drought and
527 pluvial-length, decadal timescales. To help address the resolution limitations of the proxy
528 SST data, we treated the drought and pluvial as (separate) composites. These averages
529 however, tend to reflect the broad periods when most of the drought and pluvial events
530 occurred. Nonetheless, there are important differences between drought and pluvial
531 periods. Overall, the SST reconstructions suggest that droughts and pluvials in WNA tend
532 to have La Niña-like and El Niño-like background conditions, respectively (Fig. 7c-d).
533 Proxy SST anomalies in the North Atlantic warm during WNA droughts (Fig. 7c). This
534 contrasts with the overall MCA, which has stronger warming in the North and Eastern
535 Atlantic and variable SSTs in the Western Atlantic. Pluvials in WNA are associated
536 with cooling especially in the North and Eastern Atlantic, but warming in the Gulf of
537 Mexico (Fig. 7d).

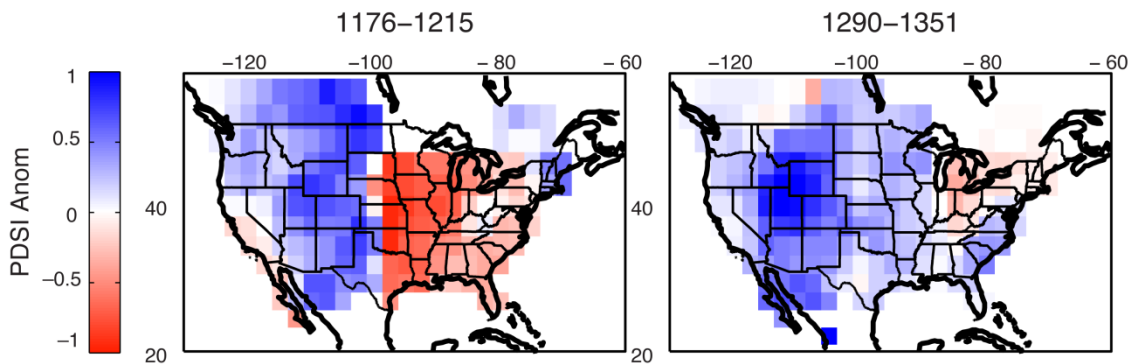
538

539 *4.3. Do SST/pluvial associations vary with multidecadal variability, for example, within*
540 *the MCA?*

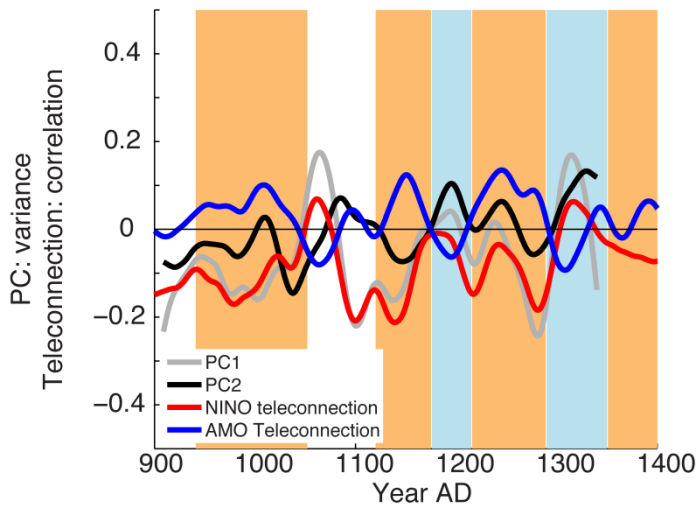
541 Our third research question addresses the two pluvials that occurred in WNA
542 during the MCA between 1176-1215 and 1290-1350 respectively. How could MCA
543 pluvials occur during a time where SST proxy records show persistent La Niña
544 conditions in the Pacific? This could partially be due to the low temporal resolution of the
545 SST proxy data, but these pluvials may also be a manifestation of the complexities in the
546 tropical Pacific SST and precipitation proxies we assessed. The two pluvials are
547 pronounced in the WNA PDSI average, and are widespread across the region (Fig. 3).

548

549 Composite maps of PDSI averaged across the years of the two pluvials show they
550 have relatively different spatial patterns across North America (Fig. 9). The earlier
551 pluvial is characterized by a strong east-west dipole, where WNA is wet and eastern
552 North America is dry. The smoothed NINO3 teleconnection series is neutral during this
553 early pluvial and the smoothed AMO teleconnection series is only slightly negative (Fig.
554 10). The east-west dipole pattern of the 1176-1215 pluvial (Fig. 9) is strikingly
555 reminiscent of the second mode of North American drought variability identified by
556 Woodhouse et al. (2009). Their first mode defined by the first principal component (PC1)
557 of the NADA reflects an ENSO type north-south dipole pattern, and their second mode
558 (PC2) reflects an east-west dipole they link to the position and sinuosity of the polar jet
559 stream and the Northern Hemispheric annular mode (NAM). During the early 1176-1215
560 pluvial, PC2 has a positive anomaly, linking the potential cause of this event to the NAM,
561 characterized by variations in patterns of atmospheric pressure (Fig. 10).



562
563 **Fig. 9.** Medieval pluvials. Reconstructed PDSI maps for MCA pluvials including the
564 1176-1215 AD and 1290-1351 AD events. Anomalies are computed with respect to the
565 900-2007 AD mean.



566

567 **Fig. 10.** Potential drivers of MCA pluvials. The MCA pluvial intervals are delineated by
 568 the vertical blue bars. The leading principal components of WNA PDSI from Woodhouse
 569 et al., 2009 are shown in grey (PC1) and black (PC2). NINO3 and AMO teleconnection
 570 strength time series are shown in red and blue respectively (this study). All series are
 571 smoothed with a 50-year cubic smoothing spline. The units for the PCs are in variance
 572 and the units for the teleconnection time series are in r-value correlation and plotted on
 573 the same axis. The first pluvial shows a positive, albeit weak, PC2 anomaly and a
 574 similarly weak negative AMO anomaly. The second pluvial shows a combination of
 575 potential forcing mechanisms, including El Niño-like and negative AMO-
 576 like teleconnection patterns, positive, or El Niño-like PC1, and a positive NAM type PC2.

577

578 The later pluvial (1290-1350) had a widespread pattern, spanning much of the
 579 continent, with the largest anomalies centered directly in the middle of WNA (Fig. 9).
 580 The widespread pattern of the second MCA pluvial is reminiscent of the AMO
 581 teleconnection pattern. The unsmoothed AMO teleconnection time series has a sequence
 582 of negative years from 1296 AD, through 1305 AD. The smoothed series in Fig. 10

583 alsoshows the AMO was negative during the earlier portion of this pluvial, suggesting
584 that the AMO may have played a role in causing the second MCA pluvial. The drought
585 modes (Woodhouse et al., 2009) are less clear during the second MCA pluvial, showing
586 anomalies in both PC1 and PC2. Together the evidence suggests MCA pluvials were
587 forced by a combination of factors, which likely included the NAM during the first
588 pluvial and perhaps North Atlantic SST variability during the second pluvial. In both
589 cases the pluvials are consistent with known mechanisms *and* the presence of La Niña-
590 like conditions in the tropical Pacific. Notably, neither pluvial map has a characteristic
591 ENSO dipole pattern when averaged across the entire pluvial duration (Fig. 9), which
592 was also true during the early 20th century pluvial (Woodhouse et al., 2005).

593

594 **5. Conclusion**

595 Reassessing the evidence linking SSTs to climate over the past millennium
596 reveals both complexities and insights into the forcing mechanisms of WNA
597 hydroclimate variability. Consistent with previous researchers (e.g., Conroy et al., 2009a;
598 Feng et al., 2008, 2010;Graham et al., 2007; Herweijer et al., 2007; Oglesby et al., 2012;
599 Seager et al., 2007), our analysis shows centennial-scale shifts in drought/pluvial
600 frequency and persistence observed between the MCA and post-MCAwere accompanied
601 by SST background changes from a La Niña-like Pacific and warm North Atlantic to an
602 El Niño-like Pacific and cold North Atlantic. The large compilation of SST
603 reconstructions presented here show the eastern North Atlantic and western tropical
604 Pacific have the most agreement and strongest signal among the SST proxy records.
605 Additional evidence, such as precipitation reconstructions, suggest MCA/post-MCA

606 conditions in the tropical Pacific were complex, and likely more nuanced than suggested
607 by the background SSTs alone. Furthermore, teleconnection patterns preserved in WNA
608 tree-ring reconstructed PDSI maps show little evidence that La Niña teleconnections
609 were more frequent during the MCA, but the strength of AMO teleconnections increased
610 somewhat. If more persistent or frequent La Niña conditions forced WNA MCA climate,
611 the teleconnection fingerprint may have been different. The difference in results for the
612 SST proxy data and the tree-ring based teleconnection patterns may also be due in part to
613 the different scales of spatial and temporal variability captured by these different types of
614 climate proxy records.

615 Teleconnection patterns suggest both the Pacific and Atlantic likely played a role
616 in forcing persistent WNA droughts and pluvials over the past millennium. The driest
617 years within droughts and the wettest years within pluvials had stronger teleconnection
618 patterns than the events as a whole. Iconic droughts like the 16th century megadrought and
619 some medieval droughts had sequences of La Niña teleconnection patterns, implicating
620 the tropical Pacific as a causal mechanism. More wide-spread events, characteristic
621 during the MCA, have stronger correlations to the AMO teleconnection pattern.

622 Reconstructed SST patterns indicate La Niña-like conditions in the Pacific and warm
623 North Atlantic SSTs accompanied droughts, while El Niño-like conditions and cool
624 North Atlantic SSTs accompanied pluvials. These patterns in-part reflect the broader
625 MCA/post-MCA SST patterns during which most of the droughts and pluvials occurred
626 respectively.

627 Finally, two MCA pluvials appear to have been forced by separate
628 mechanisms. The earlier pluvial had a spatial pattern associated with the NAM, while the

629 widespread pattern of the later pluvial has a stronger relationship with the North Atlantic
630 teleconnection pattern. Neither of these hypothesized mechanisms are inconsistent with a
631 La-Niña like Pacific, underscoring that SST background conditions alone cannot explain
632 WNA hydroclimate.

633

634 **Acknowledgements**

635 We thank the National Oceanic and Atmospheric Administration (NOAA,
636 NA11OAR4310162), the National Science Foundation (AGS1243125), the Science
637 Foundation Arizona Bisgrove Scholars Fellowship program, the NOAA funded Climate
638 Assessment for the Southwest, the University of Arizona Department of Geoscience, and
639 the Northern Arizona University School of Earth Science and Environmental
640 Sustainability for contributing funding and support for this research. We also thank
641 reviewers Dr. Gregory McCabe and two anonymous reviewers for their time, insights,
642 and feedback.

643

644

645 **References**

646 Abrantes, F., Lebreiro, S., Rodrigues, T., Gil, I., Bartels-Jónsdóttir, H., Oliveira, P.,
647 Kissel, C., Grimalt, J.O., 2005. Shallow-marine sediment cores record climate
648 variability and earthquake activity off Lisbon (Portugal) for the last 2000 years.
649 Quaternary Science Reviews 24, 2477–2494. doi:10.1016/j.quascirev.2004.04.009
650 Batehup, R., McGregor, S., Gallant, A., 2015. The influence of non-stationary ENSO
651 teleconnections on reconstructions of paleoclimate using a pseudoproxy

652 framework. *Climate of the Past Discussions* 11, 3853–3895. doi:10.5194/cpd-11-
653 3853-2015

654 Black, D.E., Abahazi, M.A., Thunell, R.C., Kaplan, A., Tappa, E.J., Peterson, L.C., 2007.
655 An 8-century tropical Atlantic SST record from the Cariaco Basin: Baseline
656 variability, twentieth-century warming, and Atlantic hurricane frequency.
657 *Paleoceanography* 22, PA4204. doi:10.1029/2007PA001427

658 Bonnet, S., de Vernal, A., Hillaire-Marcel, C., Radi, T., Husum, K., 2010. Variability of
659 sea-surface temperature and sea-ice cover in the Fram Strait over the last two
660 millennia. *Marine Micropaleontology* 74, 59–74.
661 doi:10.1016/j.marmicro.2009.12.001

662 Burgman, R., Seager, R., Clement, A., Herweijer, C., 2010. Role of tropical Pacific SSTs
663 in global medieval hydroclimate: A modeling study. *Geophys. Res. Lett.* 37,
664 L06705. doi:10.1029/2009GL042239

665 Cayan, D.R., Redmond, K.T., Riddle, L.G., 1999. ENSO and hydrologic extremes in the
666 western United States. *J. Climate* 12, 2881–2893. doi:10.1175/1520-
667 0442(1999)012<2881:EAHEIT>2.0.CO;2

668 Cobb, K.M., Charles, C.D., Cheng, H., Edwards, R.L., 2003. El Niño/Southern
669 Oscillation and tropical Pacific climate during the last millennium. *Nature* 424,
670 271–276. doi:10.1038/nature01779

671 Cole, J.E., Cook, E.R., 1998. The changing relationship between ENSO variability and
672 moisture balance in the continental United States. *Geophys. Res. Lett.* 25, 4529–
673 4532. doi:10.1029/1998GL900145

674 Conroy, J.L., Overpeck, J.T., Cole, J.E., Shanahan, T.M., Steinitz-Kannan, M., 2008.
675 Holocene changes in eastern tropical Pacific climate inferred from a Galápagos
676 lake sediment record. *Quaternary Science Reviews* 27, 1166–1180.
677 doi:10.1016/j.quascirev.2008.02.015

678 Conroy, J.L., Overpeck, J.T., Cole, J.E., Steinitz-Kannan, M., 2009a. Variable oceanic
679 influences on western North American drought over the last 1200 years. *Geophys.*
680 *Res. Lett.* 36, L17703. doi:10.1029/2009GL039558

681 Conroy, J.L., Restrepo, A., Overpeck, J.T., Steinitz-Kannan, M., Cole, J.E., Bush, M.B.,
682 Colinvaux, P.A., 2009b. Unprecedented recent warming of surface temperatures
683 in the eastern tropical Pacific Ocean. *Nature Geosci* 2, 46–50.
684 doi:10.1038/ngeo390

685 Conroy, J.L., Overpeck, J.T., Cole, J.E., 2010. El Niño/Southern Oscillation and changes
686 in the zonal gradient of tropical Pacific sea surface temperature over the last 1.2
687 ka. *PAGES* 18.

688 Cook, B.I., Smerdon, J.E., Seager, R., Cook, E.R., 2014. Pan-continental droughts in
689 North America over the last millennium. *J. Climate* 27, 383–397.
690 doi:10.1175/JCLI-D-13-00100.1

691 Cook, B.I., Cook, E.R., Anchukaitis, K.J., Seager, R., Miller, R.L., 2010. Forced and
692 unforced variability of twentieth century North American droughts and pluvials.
693 *Clim Dyn* 37, 1097–1110. doi:10.1007/s00382-010-0897-9

694 Cook, E.R., Briffa, K.R., Meko, D.M., Graybill, D.A., Funkhouser, G., 1995. The
695 “segment length curse” in long tree-ring chronology development for

696 palaeoclimatic studies. *The Holocene* 5, 229–237.
697 doi:10.1177/095968369500500211

698 Cook, E.R., Krusic, P.J., 2008. North American summer PDSI reconstructions, version
699 2a. IGBP PAGES/World Data Center for Paleoclimatology Data Contribution
700 Series 46, 2008.

701 Cook, E.R., Seager, R., Cane, M.A., Stahle, D.W., 2007. North American drought:
702 Reconstructions, causes, and consequences. *Earth-Science Reviews* 81, 93–134.
703 doi:10.1016/j.earscirev.2006.12.002

704 Cook, E.R., Seager, R., Heim, R.R., Vose, R.S., Herweijer, C., Woodhouse, C., 2010.
705 Megadroughts in North America: placing IPCC projections of hydroclimatic
706 change in a long-term palaeoclimate context. *J. Quaternary Sci.* 25, 48–61.
707 doi:10.1002/jqs.1303

708 Cook, E.R., Woodhouse, C.A., Eakin, C.M., Meko, D.M., Stahle, D.W., 2004. Long-term
709 aridity changes in the western United States. *Science* 306, 1015–1018.
710 doi:10.1126/science.1102586

711 Cronin, T.M., Dwyer, G.S., Kamiya, T., Schwede, S., Willard, D.A., 2003. Medieval
712 Warm Period, Little Ice Age and 20th century temperature variability from
713 Chesapeake Bay. *Global and Planetary Change* 36, 17–29. doi:10.1016/S0921-
714 8181(02)00161-3

715 Doose-Rolinski, H., Rogalla, U., Scheeder, G., Lückge, A., von Rad, U., 2001. High-
716 resolution temperature and evaporation changes during the Late Holocene in the
717 northeastern Arabian Sea. *Paleoceanography* 16, 358–367.
718 doi:10.1029/2000PA000511

719 Eiríksson, J., Bartels-Jónsdóttir, H.B., Cage, A.G., Gudmundsdóttir, E.R., Klitgaard-
720 Kristensen, D., Marret, F., Rodrigues, T., Abrantes, F., Austin, W.E.N., Jiang, H.,
721 Knudsen, K.-L., Sejrup, H.-P., 2006. Variability of the North Atlantic Current
722 during the last 2000 years based on shelf bottom water and sea surface
723 temperatures along an open ocean/shallow marine transect in western Europe. *The*
724 *Holocene* 16, 1017–1029. doi:10.1177/0959683606h1991rp

725 Emeis, K.-C., Dawson, A.G., 2003. Holocene palaeoclimate records over Europe and the
726 North Atlantic. *The Holocene* 13, 305–309. doi:10.1191/0959683603h1622ed

727 Emile-Geay, J., Cobb, K.M., Mann, M.E., Wittenberg, A.T., 2013. Estimating central
728 equatorial Pacific SST variability over the past millennium. Part II:
729 Reconstructions and implications. *J. Climate* 26, 2329–2352. doi:10.1175/JCLI-
730 D-11-00511.1

731 Feng, S., Hu, Q., Oglesby, R.J., 2010. Influence of Atlantic sea surface temperatures on
732 persistent drought in North America. *Clim Dyn* 37, 569–586.
733 doi:10.1007/s00382-010-0835-x

734 Feng, S., Oglesby, R.J., Rowe, C.M., Loope, D.B., Hu, Q., 2008. Atlantic and Pacific
735 SST influences on Medieval drought in North America simulated by the
736 Community Atmospheric Model. *J. Geophys. Res.* 113, D11101.
737 doi:10.1029/2007JD009347

738 Goni, M.A., Thunell, R.C., Woodworth, M.P., Müller-Karger, F.E., 2006. Changes in
739 wind-driven upwelling during the last three centuries: Interocean teleconnections.
740 *Geophys. Res. Lett.* 33, L15604. doi:10.1029/2006GL026415

741 Graham, N.E., Hughes, M.K., Ammann, C.M., Cobb, K.M., Hoerling, M.P., Kennett,
742 D.J., Kennett, J.P., Rein, B., Stott, L., Wigand, P.E., Xu, T., 2007. Tropical
743 Pacific – mid-latitude teleconnections in medieval times. *Climatic Change* 83,
744 241–285. doi:10.1007/s10584-007-9239-2

745 Gray, S.T., Graumlich, L.J., Betancourt, J.L., Pederson, G.T., 2004. A tree-ring based
746 reconstruction of the Atlantic Multidecadal Oscillation since 1567 A.D. *Geophys.*
747 *Res. Lett.* 31, L12205. doi:10.1029/2004GL019932

748 Gutiérrez, D., Bouloubassi, I., Sifeddine, A., Purca, S., Goubanova, K., Graco, M., Field,
749 D., Méjanelle, L., Velazco, F., Lorre, A., Salvatteci, R., Quispe, D., Vargas, G.,
750 Dewitte, B., Ortlieb, L., 2011. Coastal cooling and increased productivity in the
751 main upwelling zone off Peru since the mid-twentieth century. *Geophys. Res.*
752 *Lett.* 38, L07603. doi:10.1029/2010GL046324

753 Hendy, E.J., Gagan, M.K., Alibert, C.A., McCulloch, M.T., Lough, J.M., Isdale, P.J.,
754 2002. Abrupt decrease in tropical Pacific sea surface salinity at end of Little Ice
755 Age. *Science* 295, 1511–1514. doi:10.1126/science.1067693

756 Hendy, I.L., Dunn, L., Schimmelmann, A., Pak, D.K., 2013. Resolving varve and
757 radiocarbon chronology differences during the last 2000 years in the Santa
758 Barbara Basin sedimentary record, California. *Quaternary International*,
759 *PACLIM: Proceedings of the 25th Pacific Climate Workshop, 2011* 310, 155–
760 168. doi:10.1016/j.quaint.2012.09.006

761 Herweijer, C., Seager, R., Cook, E.R., Emile-Geay, J., 2007. North American droughts of
762 the last millennium from a gridded network of tree-ring data. *J. Climate* 20, 1353–
763 1376. doi:10.1175/JCLI4042.1

764 Hidalgo, H.G., 2004. Climate precursors of multidecadal drought variability in the
765 western United States. *Water Resour. Res.* 40, W12504.
766 doi:10.1029/2004WR003350

767 Hu, Q., Feng, S., 2001. Variations of Teleconnection of ENSO and Interannual Variation
768 in Summer Rainfall in the Central United States. *J. Climate* 14, 2469–2480.
769 doi:10.1175/1520-0442(2001)014<2469:VOTOEA>2.0.CO;2

770 Hu, Q., Feng, S., 2012. AMO- and ENSO-Driven Summertime Circulation and
771 Precipitation Variations in North America. *J. Climate* 25, 6477–6495.
772 doi:10.1175/JCLI-D-11-00520.1

773 Isono, D., Yamamoto, M., Irino, T., Oba, T., Murayama, M., Nakamura, T., Kawahata,
774 H., 2009. The 1500-year climate oscillation in the midlatitude North Pacific
775 during the Holocene. *Geology* 37, 591–594. doi:10.1130/G25667A.1

776 Kam, J., Sheffield, J., Wood, E.F., 2014. Changes in drought risk over the contiguous
777 United States (1901–2012): The influence of the Pacific and Atlantic Oceans.
778 *Geophys. Res. Lett.* 41, 2014GL060973. doi:10.1002/2014GL060973

779 Kaplan, A., Cane, M.A., Kushnir, Y., Clement, A.C., Blumenthal, M.B., Rajagopalan, B.,
780 1998. Analyses of global sea surface temperature 1856-1991. *Journal of*
781 *Geophysical Research* 103, 18. doi:10.1029/97JC01736

782 Keigwin, L.D., Sachs, J.P., Rosenthal, Y., 2003. A 1600-year history of the Labrador
783 Current off Nova Scotia. *Climate Dynamics* 21, 53–62. doi:10.1007/s00382-003-
784 0316-6

785 Kennett, D.J., Kennett, J.P., 2000. Competitive and cooperative responses to climatic
786 instability in coastal southern California. *American Antiquity* 65, 379–395.
787 doi:10.2307/2694065

788 Kim, J.-H., Rimbu, N., Lorenz, S.J., Lohmann, G., Nam, S.-I., Schouten, S., Rühlemann,
789 C., Schneider, R.R., 2004. North Pacific and North Atlantic sea-surface
790 temperature variability during the Holocene. *Quaternary Science Reviews*,
791 Holocene climate variability - a marine perspective 23, 2141–2154.
792 doi:10.1016/j.quascirev.2004.08.010

793 Kuhnert, H., Mulitza, S., 2011. Multidecadal variability and late medieval cooling of
794 near-coastal sea surface temperatures in the eastern tropical North Atlantic.
795 *Paleoceanography* 26, PA4224. doi:10.1029/2011PA002130

796 Kumar, A., Chen, M., Hoerling, M., Eischeid, J., 2013. Do extreme climate events
797 require extreme forcings? *Geophys. Res. Lett.* 40, 3440–3445.
798 doi:10.1002/grl.50657

799 Leduc, G., Schneider, R., Kim, J.-H., Lohmann, G., 2010a. Holocene and Eemian sea
800 surface temperature trends as revealed by alkenone and Mg/Ca paleothermometry.
801 *Quaternary Science Reviews* 29, 989–1004. doi:10.1016/j.quascirev.2010.01.004

802 Leduc, G., Herbert, C.T., Blanz, T., Martinez, P., Schneider, R., 2010b. Contrasting
803 evolution of sea surface temperature in the Benguela upwelling system under
804 natural and anthropogenic climate forcings. *Geophys. Res. Lett.* 37, L20705.
805 doi:10.1029/2010GL044353

806 Linsley, B.K., Rosenthal, Y., Oppo, D.W., 2010. Holocene evolution of the Indonesian
807 throughflow and the western Pacific warm pool. *Nature Geosci* 3, 578–583.
808 doi:10.1038/ngeo920

809 Lund, D.C., Curry, W., 2006. Florida Current surface temperature and salinity variability
810 during the last millennium. *Paleoceanography* 21, PA2009.
811 doi:10.1029/2005PA001218

812 Mantua, N.J., Hare, S.R., Zhang, Y., Wallace, J.M., Francis, R.C., 1997. A Pacific
813 interdecadal climate oscillation with impacts on salmon production. *Bull. Amer.*
814 *Meteor. Soc.* 78, 1069–1079. doi:10.1175/1520-
815 0477(1997)078<1069:APICOW>2.0.CO;2

816 McCabe, G.J., Betancourt, J.L., Gray, S.T., Palecki, M.A., Hidalgo, H.G., 2008.
817 Associations of multi-decadal sea-surface temperature variability with US
818 drought. *Quaternary International*, The 22nd Pacific Climate Workshop 188, 31–
819 40. doi:10.1016/j.quaint.2007.07.001

820 McCabe, G.J., Dettinger, M.D., 1999. Decadal variations in the strength of ENSO
821 teleconnections with precipitation in the western United States. *Int. J. Climatol.*
822 19, 1399–1410. doi:10.1002/(SICI)1097-0088(19991115)19:13<1399::AID-
823 JOC457>3.0.CO;2-A

824 McCabe, G.J., Palecki, M.A., Betancourt, J.L., 2004. Pacific and Atlantic Ocean
825 influences on multidecadal drought frequency in the United States. *PNAS* 101,
826 4136–4141. doi:10.1073/pnas.0306738101

827 McCabe, G.J., Wolock, D.M., 2013. Variability Common to Global Sea Surface
828 Temperatures and Runoff in the Conterminous United States. *J. Hydrometeorol* 15,
829 714–725. doi:10.1175/JHM-D-13-097.1

830 McGregor, H.V., Dima, M., Fischer, H.W., Mulitza, S., 2007. Rapid 20th-Century
831 Increase in coastal upwelling off northwest Africa. *Science* 315, 637–639.
832 doi:10.1126/science.1134839

833 Meko, D.M., Woodhouse, C.A., Baisan, C.A., Knight, T., Lukas, J.J., Hughes, M.K.,
834 Salzer, M.W., 2007. Medieval drought in the upper Colorado River Basin.
835 *Geophysical research letters* 34.

836 Miettinen, A., Divine, D., Koç, N., Godtliessen, F., Hall, I.R., 2012. Multicentennial
837 variability of the sea surface temperature gradient across the subpolar North
838 Atlantic over the last 2.8 kyr. *J. Climate* 25, 4205–4219. doi:10.1175/JCLI-D-11-
839 00581.1

840 Mohtadi, M., Romero, O.E., Kaiser, J., Hebbeln, D., 2007. Cooling of the southern high
841 latitudes during the Medieval Period and its effect on ENSO. *Quaternary Science*
842 *Reviews* 26, 1055–1066. doi:10.1016/j.quascirev.2006.12.008

843 Moreno, A., Pérez, A., Frigola, J., Nieto-Moreno, V., Rodrigo-Gámiz, M., Martrat, B.,
844 González-Sampériz, P., Morellón, M., Martín-Puertas, C., Corella, J.P., Belmonte,
845 Á., Sancho, C., Cacho, I., Herrera, G., Canals, M., Grimalt, J.O., Jiménez-Espejo,
846 F., Martínez-Ruiz, F., Vegas-Vilarrúbia, T., Valero-Garcés, B.L., 2012. The
847 Medieval Climate Anomaly in the Iberian Peninsula reconstructed from marine
848 and lake records. *Quaternary Science Reviews* 43, 16–32.
849 doi:10.1016/j.quascirev.2012.04.007

850 Newman, M., Compo, G.P., Alexander, M.A., 2003. ENSO-forced variability of the
851 Pacific Decadal Oscillation. *J. Climate* 16, 3853–3857. doi:10.1175/1520-
852 0442(2003)016<3853:EVOTPD>2.0.CO;2

853 Newton, A., Thunell, R., Stott, L., 2011. Changes in the Indonesian Throughflow during
854 the past 2000 yr. *Geology* 39, 63–66. doi:10.1130/G31421.1

855 Newton, A., Thunell, R., Stott, L., 2006. Climate and hydrographic variability in the
856 Indo-Pacific Warm Pool during the last millennium. *Geophys. Res. Lett.* 33,
857 L19710. doi:10.1029/2006GL027234

858 Nieto-Moreno, V., Martínez-Ruiz, F., Willmott, V., García-Orellana, J., Masqué, P.,
859 Sinninghe Damsté, J.S., 2013. Climate conditions in the westernmost
860 Mediterranean over the last two millennia: An integrated biomarker approach.
861 *Organic Geochemistry* 55, 1–10. doi:10.1016/j.orggeochem.2012.11.001

862 Nowak, K., Hoerling, M., Rajagopalan, B., Zagana, E., 2012. Colorado River Basin
863 hydroclimatic variability. *J. Climate* 25, 4389–4403. doi:10.1175/JCLI-D-11-
864 00406.1

865 Oglesby, R., Feng, S., Hu, Q., Rowe, C., 2012. The role of the Atlantic Multidecadal
866 Oscillation on medieval drought in North America: Synthesizing results from
867 proxy data and climate models. *Global and Planetary Change, Perspectives on
868 Climate in Medieval Time* 84–85, 56–65. doi:10.1016/j.gloplacha.2011.07.005

869 Oppo, D.W., Rosenthal, Y., Linsley, B.K., 2009. 2,000-year-long temperature and
870 hydrology reconstructions from the Indo-Pacific warm pool. *Nature* 460, 1113–
871 1116. doi:10.1038/nature08233

872 Palmer, W.C., 1965. Meteorological Drought. Research Paper. U.S. Weather Bureau,
873 Office of Climatology, Washington, D.C.

874 Redmond, K.T., Koch, R.W., 1991. Surface climate and streamflow variability in the
875 Western United States and their relationship to large-scale circulation indices.
876 Water Resour. Res. 27, 2381–2399. doi:10.1029/91WR00690

877 Reynolds, R.W., Rayner, N.A., Smith, T.M., Stokes, D.C., Wang, W., 2002. An
878 improved in situ and satellite SST analysis for climate. J. Climate 15, 1609–1625.
879 doi:10.1175/1520-0442(2002)015<1609:AIISAS>2.0.CO;2

880 Richey, J.N., Poore, R.Z., Flower, B.P., Quinn, T.M., 2007. 1400 yr multiproxy record of
881 climate variability from the northern Gulf of Mexico. Geology 35, 423–426.
882 doi:10.1130/G23507A.1

883 Richey, J.N., Poore, R.Z., Flower, B.P., Quinn, T.M., Hollander, D.J., 2009. Regionally
884 coherent Little Ice Age cooling in the Atlantic Warm Pool. Geophys. Res. Lett.
885 36, L21703. doi:10.1029/2009GL040445

886 Richter, T.O., Peeters, F.J.C., van Weering, T.C.E., 2009. Late Holocene (0–2.4 ka BP)
887 surface water temperature and salinity variability, Feni Drift, NE Atlantic Ocean.
888 Quaternary Science Reviews 28, 1941–1955. doi:10.1016/j.quascirev.2009.04.008

889 Rodrigues, T., Grimalt, J.O., Abrantes, F.G., Flores, J.A., Lebreiro, S.M., 2009. Holocene
890 interdependences of changes in sea surface temperature, productivity, and fluvial
891 inputs in the Iberian continental shelf (Tagus mud patch). Geochem. Geophys.
892 Geosyst. 10, Q07U06. doi:10.1029/2008GC002367

893 Routson, C.C., Woodhouse, C.A., Overpeck, J.T., 2011. Second century megadrought in
894 the Rio Grande headwaters, Colorado: How unusual was medieval drought?
895 *Geophys. Res. Lett.* 38, L22703. doi:10.1029/2011GL050015

896 Rustic, G.T., Koutavas, A., Marchitto, T.M., Linsley, B.K., 2015. Dynamical excitation
897 of the tropical Pacific Ocean and ENSO variability by Little Ice Age cooling.
898 *Science* 350, 1537–1541. doi:10.1126/science.aac9937

899 Saenger, C., Cohen, A.L., Oppo, D.W., Halley, R.B., Carilli, J.E., 2009. Surface-
900 temperature trends and variability in the low-latitude North Atlantic since 1552.
901 *Nature Geosci* 2, 492–495. doi:10.1038/ngeo552

902 Schimmelmann, A., Hendy, I.L., Dunn, L., Pak, D.K., Lange, C.B., 2013. Revised
903 2000-year chronostratigraphy of partially varved marine sediment in Santa
904 Barbara Basin, California. *GFF* 135, 258–264.
905 doi:10.1080/11035897.2013.773066

906 Schubert, S., Gutzler, D., Wang, H., Dai, A., Delworth, T., Deser, C., Findell, K., Fu, R.,
907 Higgins, W., Hoerling, M., Kirtman, B., Koster, R., Kumar, A., Legler, D.,
908 Lettenmaier, D., Lyon, B., Magana, V., Mo, K., Nigam, S., Pegion, P., Phillips,
909 A., Pulwarty, R., Rind, D., Ruiz-Barradas, A., Schemm, J., Seager, R., Stewart,
910 R., Suarez, M., Syktus, J., Ting, M., Wang, C., Weaver, S., Zeng, N., 2009. A
911 U.S. CLIVAR project to assess and compare the responses of global climate
912 models to drought-related SST forcing patterns: overview and results. *J. Climate*
913 22, 5251–5272. doi:10.1175/2009JCLI3060.1

914 Seager, R., Burgman, R., Kushnir, Y., Clement, A., Cook, E., Naik, N., Miller, J., 2008.
915 Tropical Pacific forcing of North American medieval megadroughts: Testing the

916 concept with an atmosphere model forced by coral-reconstructed SSTs. *J. Climate*
917 21, 6175–6190. doi:10.1175/2008JCLI2170.1

918 Seager, R., Goddard, L., Nakamura, J., Henderson, N., Lee, D.E., 2014. Dynamical
919 causes of the 2010/11 Texas–Northern Mexico drought. *J. Hydrometeor* 15, 39–
920 68. doi:10.1175/JHM-D-13-024.1

921 Seager, R., Graham, N., Herweijer, C., Gordon, A.L., Kushnir, Y., Cook, E., 2007.
922 Blueprints for Medieval hydroclimate. *Quaternary Science Reviews* 26, 2322–
923 2336. doi:10.1016/j.quascirev.2007.04.020

924 Seager, R., Kushnir, Y., Herweijer, C., Naik, N., Velez, J., 2005. Modeling of Tropical
925 Forcing of Persistent Droughts and Pluvials over Western North America: 1856–
926 2000. *J. Climate* 18, 4065–4088. doi:10.1175/JCLI3522.1

927 Sepúlveda, J., Pantoja, S., Hughen, K.A., Bertrand, S., Figueroa, D., León, T., Drenzek,
928 N.J., Lange, C., 2009. Late Holocene sea-surface temperature and precipitation
929 variability in northern Patagonia, Chile (Jacaf Fjord, 44°S). *Quaternary Research*
930 72, 400–409. doi:10.1016/j.yqres.2009.06.010

931 Sicre, M.-A., Hall, I.R., Mignot, J., Khodri, M., Ezat, U., Truong, M.-X., Eiríksson, J.,
932 Knudsen, K.-L., 2011. Sea surface temperature variability in the subpolar Atlantic
933 over the last two millennia. *Paleoceanography* 26, PA4218.
934 doi:10.1029/2011PA002169

935 Sicre, M.-A., Yiou, P., Eiríksson, J., Ezat, U., Guimbaut, E., Dahhaoui, I., Knudsen, K.-
936 L., Jansen, E., Turon, J.-L., 2008. A 4500-year reconstruction of sea surface
937 temperature variability at decadal time-scales off North Iceland. *Quaternary*
938 *Science Reviews* 27, 2041–2047. doi:10.1016/j.quascirev.2008.08.009

939 Spielhagen, R.F., Werner, K., Sørensen, S.A., Zamelczyk, K., Kandiano, E., Budeus, G.,
940 Husum, K., Marchitto, T.M., Hald, M., 2011. Enhanced modern heat transfer to
941 the Arctic by warm Atlantic water. *Science* 331, 450–453.
942 doi:10.1126/science.1197397

943 St. George, S., Meko, D.M., Cook, E.R., 2010. The seasonality of precipitation signals
944 embedded within the North American Drought Atlas. *The Holocene*.
945 doi:10.1177/0959683610365937

946 Stott, L., Cannariato, K., Thunell, R., Haug, G.H., Koutavas, A., Lund, S., 2004. Decline
947 of surface temperature and salinity in the western tropical Pacific Ocean in the
948 Holocene epoch. *Nature* 431, 56–59. doi:10.1038/nature02903

949 van Oldenborgh, G.J., Te Raa, L., Dijkstra, H., Philip, S., 2010. Frequency- or amplitude-
950 dependent effects of the Atlantic meridional overturning on the tropical Pacific
951 Ocean. Presented at the EGU General Assembly Conference Abstracts, p. 5755.

952 Thomson, D.J., 1982. Spectrum estimation and harmonic analysis. *Proceedings of the*
953 *IEEE* 70, 1055–1096. doi:10.1109/PROC.1982.12433

954 Tierney, J.E., Oppo, D.W., Rosenthal, Y., Russell, J.M., Linsley, B.K., 2010.
955 Coordinated hydrological regimes in the Indo-Pacific region during the past two
956 millennia. *Paleoceanography* 25, PA1102. doi:10.1029/2009PA001871

957 Tootle, G.A., Piechota, T.C., Singh, A., 2005. Coupled oceanic-atmospheric variability
958 and U.S. streamflow. *Water Resour. Res.* 41, W12408.
959 doi:10.1029/2005WR004381

960 Wanamaker, A.D., Kreutz, K.J., Schöne, B.R., Pettigrew, N., Borns, H.W., Introne, D.S.,
961 Belknap, D., Maasch, K.A., Feindel, S., 2007. Coupled North Atlantic slope water

962 forcing on Gulf of Maine temperatures over the past millennium. *Clim Dyn* 31,
963 183–194. doi:10.1007/s00382-007-0344-8

964 Wang, H., Mehta, V.M., 2008. Decadal variability of the Indo-Pacific Warm Pool and its
965 association with atmospheric and oceanic variability in the NCEP–NCAR and
966 SODA reanalyses. *J. Climate* 21, 5545–5565. doi:10.1175/2008JCLI2049.1

967 Wang, S.-Y., Hipps, L., Gillies, R.R., Yoon, J.-H., 2014. Probable causes of the abnormal
968 ridge accompanying the 2013–2014 California drought: ENSO precursor and
969 anthropogenic warming footprint. *Geophys. Res. Lett.* 41, 2014GL059748.
970 doi:10.1002/2014GL059748

971 Woodhouse, C.A., Kunkel, K.E., Easterling, D.R., Cook, E.R., 2005. The twentieth-
972 century pluvial in the western United States. *Geophys. Res. Lett.* 32, L07701.
973 doi:10.1029/2005GL022413

974 Woodhouse, C.A., Overpeck, J.T., 1998. 2000 Years of drought variability in the central
975 United States. *Bull. Amer. Meteor. Soc.* 79, 2693–2714. doi:10.1175/1520-
976 0477(1998)079<2693:YODVIT>2.0.CO;2

977 Woodhouse, C.A., Russell, J.L., Cook, E.R., 2009. Two modes of North American
978 Drought from instrumental and paleoclimatic data. *J. Climate* 22, 4336–4347.
979 doi:10.1175/2009JCLI2705.1

980 Wu, W., Tan, W., Zhou, L., Yang, H., Xu, Y., 2012. Sea surface temperature variability
981 in southern Okinawa Trough during last 2700 years. *Geophys. Res. Lett.* 39,
982 L14705. doi:10.1029/2012GL052749

983 Yan, H., Sun, L., Wang, Y., Huang, W., Qiu, S., Yang, C., 2011. A record of the
984 Southern Oscillation Index for the past 2,000 years from precipitation proxies.
985 Nature Geosci 4, 611–614. doi:10.1038/ngeo1231

986 Zhao, M., Eglinton, G., Read, G., Schimmelmann, A., 2000. An alkenone (U37K') quasi-
987 annual sea surface temperature record (A.D. 1440 to 1940) using varved
988 sediments from the Santa Barbara Basin. Organic Geochemistry 31, 903–917.
989 doi:10.1016/S0146-6380(00)00034-6